
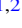






Probing the Time Variation of a Fine Structure Constant Using Galaxy Clusters and the Quintessence Model

Zhi-E Liu (刘志娥)¹ , Wen-Fei Liu (刘文斐)¹, Tong-Jie Zhang (张同杰)^{1,2} , Zhong-Xu Zhai (翟忠旭)³ , and Kamal Bora⁴ 

¹ College of Physics and Electronic Engineering, Qilu Normal University Jinan 250200, People's Republic of China; zhieliu@163.com, tjzhang@bnu.edu.cn

² Department of Astronomy, Beijing Normal University Beijing 100875, People's Republic of China

³ IPAC, California Institute of Technology Mail Code 314-6, 1200 E. California Blvd., Pasadena, CA 91125, USA

⁴ Department of Physics, Indian Institute of Technology Hyderabad, Kandi, Telangana-502284, India

Received 2021 June 18; revised 2021 August 22; accepted 2021 August 24; published 2021 November 16

Abstract

We explore a possible time variation of the fine structure constant ($\alpha \equiv e^2/\hbar c$) using the Sunyaev–Zel’dovich effect measurements of galaxy clusters along with their X-ray observations. Specifically, the ratio of the integrated Comptonization parameter $Y_{SZ}D_A^2$ and its X-ray counterpart Y_X is used as an observable to constrain the bounds on the variation of α . Considering the violation of the cosmic distance duality relation, this ratio depends on the fine structure constant of $\sim \alpha^3$. We use the quintessence model to provide the origin of α time variation. In order to give a robust test on α variation, two galaxy cluster samples, the 61 clusters provided by the Planck collaboration and the 58 clusters detected by the South Pole Telescope (SPT), are collected for analysis. Their X-ray observations are given by the XMM-Newton survey. Our results give $\zeta = -0.203_{-0.099}^{+0.101}$ for the Planck sample and $\zeta = -0.043_{-0.148}^{+0.165}$ for the SPT sample, indicating that α is constant with redshift within 3σ and 1σ for the two samples, respectively.

Unified Astronomy Thesaurus concepts: Quintessence (1323); Cosmological models (337); Galaxy clusters (584)

1. Introduction

The fine structure constant $\alpha \equiv e^2/\hbar c$ is at the central position in the system of fundamental physical constants. It measures the strength of the electromagnetic interaction between charged elementary particles in the low-energy limit. Recently, the fine structure constant was determined at an unprecedented precise measurement, that is, $\alpha^{-1} = 137.035999206$ with a relative accuracy of 81 parts per trillion (Morel et al. 2020). However, in 1937, Dirac (1937) argued that the fundamental constants of nature may not be pure constants but may vary slowly with the epoch, and he proposed a gravitational constant decreasing proportionally to t^{-1} . Since then, some theoretical and experimental investigations allowing spacetime variation of fundamental constants have been put into effect (Uzan 2011, 2003; Martins 2017; Wang & Chen 2020). In order to remedy the dire consequence (Teller 1948) induced by the varying gravitational constant $G \sim t^{-1}$, Gamow (1967) suggested that e^2 increases in direct proportion to the age of the universe. Phenomenological models that usually assumed an α varying as some power law or logarithm of time, like those introduced by Gamow, represent the early work of studying varying α (Barrow & Tipler 1986).

Over the last few decades, the focus has shifted to various extensions of standard models, in which one or more fundamental constants of nature become dynamical quantities. The first self-consistent theory of varying α is the framework constructed by Bekenstein (1982) via modifying Maxwell electrodynamics, which was then extended to a cosmological setting by Sandvik et al. (2002), Barrow et al. (2002b), Barrow & Mota (2003), and Barrow et al. (2002a), namely the BSBM theory. In the BSBM model, variations in α occur due to a coupling between the electromagnetic field and a massless scalar field in the action. The original BSBM model was then extended by adding a nontrivial potential (Barrow & Li 2008; Farajollahi & Salehi 2012), or by allowing the coupling between scalar field ϕ and photons as a function of ϕ

(Barrow & Lip 2012), or by allowing for both an arbitrary coupling and potential function (Barrow & Graham 2013). Another class of the extensions of standard models is based on the belief that space has more than three-dimensions, and the extra space dimensions can cause varying fundamental constants (Chodos & Detweiler 1980; Marciano 1984; Kolb et al. 1986; Barrow 1987). For instance, in Kaluza–Klein (KK) theories, the time evolution of the mean KK radius R_{KK} of extra spatial dimensions can give rise to time variations of fundamental constants (Marciano 1984).

At present, observational data of α variation are becoming increasingly abundant. The cosmic microwave background (CMB) data (O’Bryan et al. 2015; PLANCK Collaboration 2015; Hart & Chluba 2018) and the big bang nucleosynthesis (BBN; Iocco et al. 2009; Mosquera & Civitaresse 2013; Clara & Martins 2020) can constrain α variations in the early universe. The Planck Collaboration (2015) obtained $\Delta\alpha/\alpha \approx 10^{-3}$ at a redshift of $z \approx 10^3$ by analyzing the CMB spectra, and the constraints given by the abundance of the light elements emerged during BBN are not very tight (approximately $\Delta\alpha/\alpha < 10^{-2}-10^{-3}$ at $z \approx 10^9-10^{10}$), too (Mosquera & Civitaresse 2013). The 1.8 billion-year-old natural nuclear reactor at the Oklo Uranium Mine in Gabon can give much tighter bounds on the time variations of α ($\Delta\alpha/\alpha \approx 10^{-7}-10^{-8}$; Damour & Dyson 1996; Lamoreaux & Torgerson 2004). The most sensitive constraints on $\Delta\alpha/\alpha$ were achieved at $z \approx 1-6$ from the spectral lines significantly affected by relativistic effects in absorbing clouds around distant quasars. The quasar absorption lines observed by Keck/High Resolution Echelle Spectrometer (HIRES) and Very Large Telescope (VLT)/Ultraviolet and Visual Echelle Spectrograph (UVES) telescopes have produced a large data sample that describes the dependence of $\Delta\alpha/\alpha$ on redshift z , in which the variations of α are normally constrained by $\Delta\alpha/\alpha \approx 10^{-5}-10^{-6}$ (Murphy et al. 2001a, 2001b, 2001c, 2003, 2004, 2007, 2008; Chand et al. 2004; Srianand et al. 2004; Webb et al. 1999, 2001). In addition, the spatial variations of α observed by comparing the results from

Keck and VLT are of interest to study. Specifically, at $z > 1.8$ the northern sky observations of the Keck telescope suggested a smaller value of the fine structure constant ($\Delta\alpha/\alpha = (-0.74 \pm 0.17) \times 10^{-5}$), but the southern sky observations of the VLT telescope showed an increasing fine structure constant ($\Delta\alpha/\alpha = (0.61 \pm 0.20) \times 10^{-5}$; Webb et al. 2011; King et al. 2012). This could be due to undetected systematic effects, but may also hint to new physics. More recently, a constraint on the relative variation of α below 10^{-5} is obtained by comparing the absorption lines of late-type evolved giant stars from the S-star cluster orbiting the supermassive black hole in our Galactic center with the absorption lines in the lab (Hees et al. 2020). The absorption lines of white dwarf stars can also be used to constrain $\Delta\alpha/\alpha$ (Berengut et al. 2013).

Some work consider a class of dilaton runaway models, where $\Delta\alpha/\alpha = -\gamma \ln(1+z)$, and indirectly constrain $\Delta\alpha/\alpha$ by constraining γ . Most of this kind of work employed the observations of the Sunyaev–Zel’dovich effect (SZ effect, hereafter) combined with observations of the X-ray surface brightness of galaxy clusters, for which the former can be characterized by the integrated Comptonization parameter $Y_{SZ} D_A^2$ and the latter by the Y_X parameter (Holanda et al. 2017, 2016a, 2016b; Colaço et al. 2019; Bora & Desai 2021a, 2021b). Alternatively, Colaço et al. (2021a, 2021b) used combined measurements of strong gravitational lensing systems and Type Ia supernovae to constrain γ . Instead of basing α on runaway models, Galli (2013) assumed that α can linearly vary with redshift, i.e., $\alpha/\alpha_0 = A_{\text{lin}}(1+z)$, and then studied whether α is time-dependent by constraining A_{lin} using the SZ effect and its X-ray counterpart of galaxy clusters.

In this paper, we will consider a specific model for the variation of the fine structure constant α driven by a typical quintessence scenario, i.e., a linear coupling with the electromagnetic term in Lagrangian.

2. Coupling of the Quintessence to the Electromagnetic Field

Quintessence is a type of dynamical scalar field models (Padmanabhan 2003). It has been used to model the dark-energy component in the universe. We expect the quintessence field to couple with the electromagnetic sector of the matter–radiation Lagrangian and induce a time variation of the fine structure constant α . The general form of the action involving a quintessence scalar field and its coupling with the electromagnetic term can be written as (Marra & Rosati 2005)

$$S = \frac{1}{16\pi G} \int d^4x \sqrt{-g} R + \int d^4x \sqrt{-g} \left[\frac{1}{2} \partial^\mu \phi \partial_\mu \phi - V(\phi) \right] - \frac{1}{4} \int d^4x \sqrt{-g} B_F(\phi) F_{\mu\nu} F^{\mu\nu} + \int d^4x \sqrt{-g} \mathcal{L}, \quad (1)$$

where G is Newton’s Gravitational constant and \mathcal{L} represents the Lagrangian density including the standard model fields and a hypothetical dark matter sector. $B_F(\phi)$ describes the coupling between quintessence and the electromagnetic field and allows for the evolution in ϕ . The effective fine structure constant depends on the value of ϕ as (Copeland et al. 2004)

$$\alpha(\phi) = \frac{\alpha_0}{B_F(\phi)}, \quad (2)$$

where α_0 is the fine structure constant measured today. Therefore, we get the relative variation of α :

$$\frac{\Delta\alpha}{\alpha} \equiv \frac{\alpha(t) - \alpha_0}{\alpha_0} = \frac{1 - B_F(\phi)}{B_F(\phi)}. \quad (3)$$

We consider a homogeneous and isotropic Friedmann–Robertson–Walker (FRW) cosmology described by the line element

$$ds^2 = -dt^2 + a^2(t) \left[\frac{dr^2}{1 - Kr^2} + r^2(d\theta^2 + \sin^2\theta d\varphi^2) \right], \quad (4)$$

where $a(t)$ and K are the scale factor and spatial curvature, respectively. Combining Equations (1) and (4) can yield equations describing the evolution of the quintessence scalar field in the FRW universe, that is, the Friedmann equation (Park & Ratra 2019)

$$\left(\frac{H}{H_0} \right)^2 = \frac{1}{1 - \frac{1}{6}(\phi')^2} \left[\Omega_m a^{-3} + \Omega_r a^{-4} + \Omega_k a^{-2} + \frac{V(\phi)}{3H_0^2} \right] \quad (5)$$

and the Klein–Gordon equation (Park & Ratra 2019)

$$\phi'' + \left(3 + \frac{\dot{H}}{H^2} \right) \phi' + \frac{dV(\phi)}{d\phi} \frac{1}{H^2} = 0, \quad (6)$$

where $\phi' \equiv d\phi/d \ln a$, and an overdot denotes the time derivative d/dt . We have set the present scale factor to $a_0 = 1$ and chose the units such that the Newtonian gravitational constant $G \equiv 1/8\pi$. $H = \dot{a}/a$ is the Hubble parameter and H_0 is the Hubble constant. The present value of the nonrelativistic matter density parameter Ω_m is the sum of the present baryonic matter and the cold dark matter (CDM) density parameters, $\Omega_m = \Omega_b + \Omega_c$. Ω_r is the present value of the radiation density parameter, and Ω_k is the present value of the spatial curvature density parameter. We assume a spatially flat universe, $\Omega_k = 0$, and set $\Omega_m = 0.315 \pm 0.007$, $H_0 = 67.4 \pm 0.5 \text{ km s}^{-1} \text{ Mpc}^{-1}$ according to the Planck 2018 results (Chen et al. 2019; Planck Collaboration 2020). Ω_r is not a free parameter but is determined by $\Omega_r = \Omega_m a_{\text{eq}}$, where a_{eq} is the scale factor at the epoch of matter–radiation equality given by $a_{\text{eq}} = \frac{4.15 \times 10^{-5}}{\Omega_m h^2}$ (Dodelson & Schmidt 2020). Here $h = H_0/(100 \text{ km s}^{-1} \text{ Mpc}^{-1})$.

A general functional form of the quintessence potential $V(\phi)$ can be written as a combination of a power law and exponential functions. Copeland et al. (2004) discussed in detail the effect induced by different quintessence models on the cosmological $\Delta\alpha$. In our work, we only consider an inverse power-law potential (Peebles & Ratra 1988; Samushia & Ratra 2006, 2009; Chen & Ratra 2011; Park & Ratra 2019),

$$V(\phi) = V_1 \phi^{-n}, \quad (7)$$

where V_1 and n are non-negative constant parameters. In the limit $n=0$ the quintessence dark energy becomes the cosmological constant Λ . The exponent parameter n has been constrained to $[0, 6]$ by various observational data (Park & Ratra 2019). Marra & Rosati (2005) showed that choosing different quintessence potentials gives a subdominant effect on

the cosmological variation of α with respect to changing the coupling function $B_F(\phi)$. Our tests also show that different values of n only have a mild impact on the result, and fixing this parameter can improve the efficiency of the computation significantly. Thus, following Marra & Rosati (2005) we set $n = 1.0$ in order to have the correct attractor equation of state (Marra & Rosati 2005). By definition, the pressure p_ϕ and energy density ρ_ϕ of the scalar field are given by

$$\begin{aligned} p_\phi &= \frac{\dot{\phi}^2}{2} - V(\phi), \\ \rho_\phi &= \frac{\dot{\phi}^2}{2} + V(\phi), \end{aligned} \quad (8)$$

and the equation of state for the scalar field is $\omega_\phi = p_\phi/\rho_\phi$. The coefficient parameter V_1 of the potential of Equation (7) can be numerically calculated by making the current energy density $\rho_\phi^{(0)}$, which is evolved from Equation (6), equal to

$$\rho_{cr}\Omega_\phi = \rho_{cr}(1 - \Omega_m - \Omega_r - \Omega_k), \quad (9)$$

where $\rho_{cr} = 3H_0^2$ is the critical density. Thus, V_1 is in fact determined by n implicitly. Accordingly, the current dark-energy density parameter is $\Omega_\phi = \rho_\phi^{(0)}/\rho_{cr} = (\phi'_0)^2/6 + V(\phi_0)/(3H_0^2)$, where ϕ_0 and ϕ'_0 are the current values of ϕ and ϕ' .

We numerically solve the cosmological Equations (5)–(6) and then produce the resulting $\Delta\alpha$ at a series of redshifts. We use the initial conditions (Peebles & Ratra 1988)

$$\phi = \left[\frac{2}{3}n(n+2) \right]^{1/2} \left(\frac{a}{a_1} \right)^{3/(n+2)} \quad (10)$$

at a scale factor of $a_i = 10^{-10}$. Here a_1 denotes the characteristic epoch at which the dominant mass density switches from ordinary matter to the ϕ field.

Equation (3) shows that the evolution of α depends on the evolution of ϕ via a concrete functional form of $B_F(\phi)$, so what follows is the choice of $B_F(\phi)$. In principle, there are no constraints on the form of $B_F(\phi)$. Marra & Rosati (2005) proposed a general form of the function $B_F(\phi)$, which is characterized by a set of four parameters, and comprehensively discussed various $B_F(\phi)$ cases that gave different α histories. In this work we adopt the simplest case originally proposed by Bekenstein (1982), i.e., a linear dependence on ϕ such that

$$B_F(\phi) = 1 - \zeta(\phi - \phi_0), \quad (11)$$

where ϕ_0 denotes the present quintessence, and ζ is a parameter describing the strength of the coupling between quintessence and the electromagnetic field, which is to be determined by the observational data. The case $\zeta = 0$, or $B_F(\phi) = 1$, means there is no coupling to the electromagnetic field, and thus the fine structure constant α really remains as a constant during the lifetime of the universe. Substituting Equation (11) into Equation (3) results in

$$\frac{\Delta\alpha}{\alpha} = \zeta(\phi - \phi_0). \quad (12)$$

3. $Y_{SZ} - Y_X$ Relation and α

The Sunyaev–Zel’dovich effect (Y_{SZ}) and X-ray surface brightness (Y_X) are two observable quantities of galaxy clusters. Since Y_{SZ} and Y_X both reflect the thermal energy of the cluster and are proportional to the total cluster mass, their ratio $Y_{SZ}D_A^2/Y_X$ should be a constant independent of redshift. This ratio has been used to explore the variation of α (Galli 2013; Holanda et al. 2016b; Colaço et al. 2019; Bora & Desai 2021a, 2021b), which is also our main focus in this paper.

The high-energy electrons in the ionized intergalactic gas of galaxy clusters can scatter the CMB photons, via inverse Compton effect, resulting in the distortion of the CMB spectrum. This is the known SZ effect (Sunyaev & Zel’dovich 1972). The CMB spectral distortion caused by the SZ effect is proportional to the Compton parameter y , which is expressed as

$$y = \frac{\sigma_T k_B}{m_e c^2} \int n_e T dl = \frac{\sigma_T}{m_e c^2} \int P dl, \quad (13)$$

where k_B is the Boltzmann constant, c is the speed of light, m_e is the electron mass, n_e is the number density of electrons, T is the electron temperature, and $P = n_e k_B T$ is the pressure of the intracluster medium under the assumption of an ideal gas equation of state. Therefore, the Compton parameter quantifies the gas pressure of the intracluster medium integrated along the line of sight. The Thompson cross-section σ_T can be computed using Feynman diagrams and linked to the fine structure constant α by

$$\sigma_T = \frac{8\pi}{3} \left(\frac{e^2}{m_e c^2} \right)^2 = \frac{8\pi}{3} \left(\frac{\hbar^2 \alpha^2}{m_e^2 c^2} \right). \quad (14)$$

Integrating the Compton parameter y over the plane perpendicular to the line of sight can provide the spherical integrated Compton parameter, defined as

$$\begin{aligned} Y_{SZ} D_A^2 &= \int y dA \\ &= \frac{\sigma_T k_B}{m_e c^2} \int n_e T dl dA = \frac{\sigma_T}{m_e c^2} \int P dV. \end{aligned} \quad (15)$$

Thus, we can see that $Y_{SZ} D_A^2$ depends on the fine structure constant through the Thompson cross-section (see Equation (14)) as (Galli 2013)

$$Y_{SZ} D_A^2 \propto \alpha^2. \quad (16)$$

According to Equation (2), we have

$$Y_{SZ} D_A^2 \propto B_F^{-2}(\phi). \quad (17)$$

The intergalactic hot gas emits mainly through thermal bremsstrahlung. The magnitude of the X-ray emission is quantified by the Y_X parameter, which can be acquired by X-ray surface brightness observations, and is defined as (Kravtsov et al. 2006)

$$Y_X = M_g(R) T_X, \quad (18)$$

where $M_g(R)$ is the X-ray determined gas mass within the radius R and T_X is the X-ray temperature of the cluster. It has been shown that $M_g(R)$ can be written as (Goncalves et al. 2012;

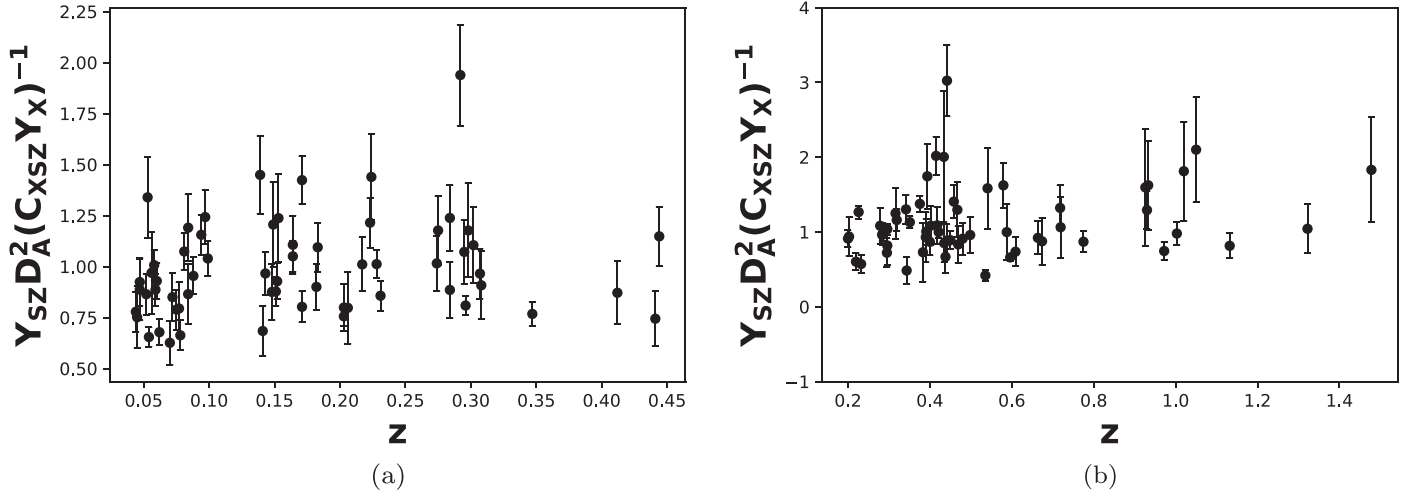


Figure 1. The observed ratio $Y_{SZ} D_A^2 / Y_X C_{XSZ}$. They are calculated from (a) the Planck galaxy cluster sample and (b) the SPT galaxy cluster sample.

Colaço et al. 2019)

$$M_g(<\theta) \propto \alpha^{-3/2} D_L D_A^{3/2}, \quad (19)$$

where D_L is the luminosity distance. This equation shows that $M_g(R)$ depends not only on the fine structure constant but also on the validity of the cosmic distance duality relation (CDDR), $D_L = (1+z)^2 D_A$. A variation of α will lead to a violation of the CDDR (Hees et al. 2014), which is normally described as $D_L = \eta(z)(1+z)^2 D_A$. Consequently, Y_X will scale to $\alpha(z)$ and $\eta(z)$ by

$$Y_X \propto M_g(<\theta) \propto \alpha(z)^{-3/2} \eta(z). \quad (20)$$

According to the scalar field theory, $\alpha(z)$ and $\eta(z)$ are linked by (Hees et al. 2014)

$$\frac{\Delta\alpha}{\alpha} \equiv \frac{\alpha(z) - \alpha_0}{\alpha_0} = \eta(z)^2 - 1. \quad (21)$$

Together with Equation (2) we have

$$Y_X \propto \alpha^{-1} \propto B_F(\phi). \quad (22)$$

Then, based on Equations (17) and (22), the dimensionless ratio of $Y_{SZ} D_A^2$ to Y_X can be related to the coupling strength $B_F(\phi)$ by

$$\frac{Y_{SZ} D_A^2}{Y_X} \propto B_F(\phi)^{-3}. \quad (23)$$

This ratio can also be expressed in the following form (Galli 2013):

$$\frac{Y_{SZ} D_A^2}{Y_X} \propto C_{XSZ} \frac{\int n_e(r) T(r) dV}{T(R) \int n_e(r) dV}, \quad (24)$$

where

$$C_{XSZ} = \frac{\sigma_T}{m_e c^2} \frac{1}{\mu_e m_p} \approx 1.416 \times 10^{-19} \left(\frac{\text{Mpc}^2}{M_\odot \text{keV}} \right). \quad (25)$$

The numerator and denominator in Equation (24) are both approximations of the thermal energy of the cluster. As discussed in Colaço et al. (2019), this ratio would be exactly constant with redshift if no new physics are assumed. As done

by Galli (2013), Colaço et al. (2019), and Bora & Desai (2021a), and considering Equation (11), we can rewrite the ratio in Equation (23) into

$$\frac{Y_{SZ} D_A^2}{Y_X C_{XSZ}} = C B_F(\phi)^{-3} = C(1 - \zeta(\phi - \phi_0))^{-3}, \quad (26)$$

where C is a constant to be determined. The case of $C \simeq 1$ indicates that the galaxy clusters used in this analysis are isothermal.

We are interested in a possible α variation as predicted by the quintessence model. The quintessence scalar field ϕ evolves via Equations (5) and (6), then the constants C and ζ can be determined by observational measurements. As shown in Equation (12), if the resulting ζ departs from zero significantly, a time variation for α should be established.

4. Galaxy Cluster Samples

Large solid angle surveys employing the SZ effect have been carried out with the South Pole Telescope (SPT; Carlstrom et al. 2011), Planck (Ade et al. 2011a), and the Atacama Cosmology Telescope (Fowler et al. 2007). One data set used here is the SZ and X-ray data extracted from Table 1 of Ade et al. (2011a). The SZ effect measurements in the direction of 62 nearby galaxy clusters ($z < 0.5$), which is a subsample of the Planck Early Sunyaev-Zel'dovich (ESZ) cluster sample (Ade et al. 2011b), were detected at a high signal-to-noise ratio ($S/N \geq 6$) in the first Planck all-sky data set. These galaxy clusters are not contaminated by flares and their morphologies are regular enough that spherical symmetry can be assumed. They had also been observed by the XMM-Newton telescope, and their Y_X measurements were obtained with the deep XMM-Newton X-ray data (Piffaretti et al. 2011). As done by Galli (2013), cluster A2034 is excluded from the analysis since its redshift estimate is discordant in Ade et al. (2011a) and Mantz et al. (2010). So we use 61 Planck ESZ clusters in this analysis covering the redshift range of $0.044 < z < 0.44$ (see Figure 1(a)). The Y_{SZ} and Y_X parameters are labeled as $D_A^2 Y_{500}$ and $Y_{X,500}$, respectively. Here 500 indicates a radius R_{500} at which the mean matter density of the cluster is 500 times that of the critical density of the universe at the redshift of the cluster. The computation of the Y_{SZ} parameter requires shaping the thermal pressure (P) of the intracluster medium for

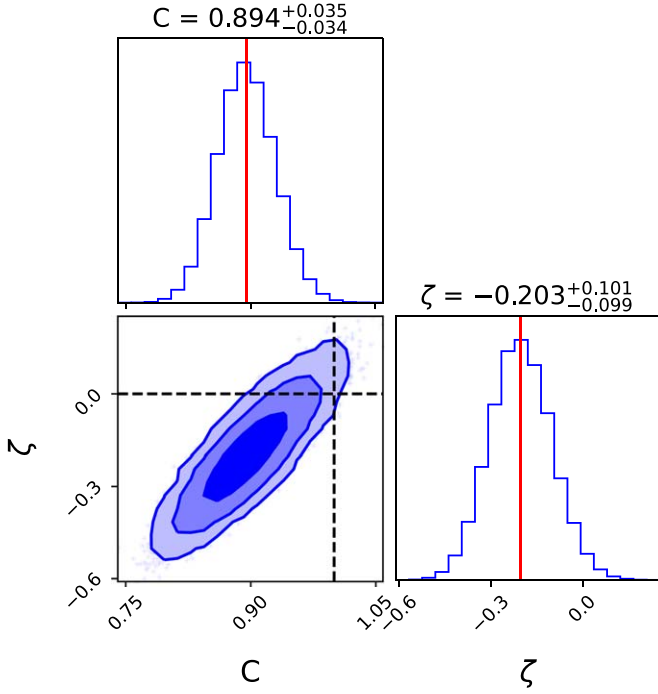


Figure 2. Contours of 1σ , 2σ , and 3σ on the $\zeta - C$ plane and the corresponding one-dimensional marginalized likelihood distributions for the Planck clusters.

each galaxy cluster by using the universal pressure profile (Arnaud et al. 2010). Furthermore, the X-ray temperatures are defined within a cylindrical annulus of radius $[0.15-0.75]R_{500}$. See Galli (2013) and Colaço et al. (2019) for more comments on the data set.

Another data set used in our analysis is the SPT galaxy cluster sample. SPT is a 10 m telescope at the South Pole that images the sky at three different frequencies, i.e., 95 GHz, 150 GHz, and 220 GHz (Carlstrom et al. 2011). SPT has detected 516 galaxy clusters via the SZ effect in the 2500 square degree SPT-SZ survey at $0 < z < 1.8$ with masses $M_{500} \geq 3 \times 10^{14} M_{\odot}$, and approximately 20% of the sample lies at $z > 0.8$ (Bleem et al. 2015). The redshifts of the SPT cluster candidates have been obtained through dedicated optical surveys and follow-up programs (Desai et al. 2012; Song et al. 2012; Saro et al. 2015). Their properties were described in Bleem et al. (2015), among which the redshift values were updated in Bocquet et al. (2019). The Y_{SZ} value of each SPT cluster is measured through integrating the thermal SZ signal in a cylindrical volume within a 0.75 -radius aperture. Note their X-ray counterpart, Y_X , is measured within a three-dimensional sphere with a radius of R_{500} . In order to compare Y_{SZ} with Y_X , one needs to convert the SPT Y_{SZ} values to spherically integrated Y_{SZ} within the same radius at which Y_X was measured. This conversion is performed based on the following expressions (Arnaud et al. 2010):

$$Y_{\text{cyl}}(R_1) = Y_{\text{sph}}(R_b) - \frac{\sigma_T}{m_e c^2} \int_{R_1}^{R_b} 4\pi P(r) \sqrt{r^2 - R_1^2} r dr \quad (27)$$

$$Y_{\text{sph}}(R_2) = \frac{\sigma_T}{m_e c^2} \int_0^{R_2} 4\pi P(r) r^2 dr. \quad (28)$$

Here, $Y_{\text{cyl}}(R_1)$ is the Y_{SZ} parameter measured within a cylindrical aperture of radius R_1 , and $Y_{\text{sph}}(R_2)$ is the Y_{SZ} parameter integrated within a spherical volume of radius R_2 . R_b is the radial extent of

the cluster, and $P(r)$ is the gas pressure in the intracluster medium. An analytical form of $P(r)$ is needed to calculate the integrations in Equations (27–28), for which we adopt the universal pressure profile suggested by Arnaud et al. (2010). Following Bora & Desai (2021a), we set $R_b = 10R_{500}$. Since the SPT observation gave Y_{SZ} values in terms of an aperture of 0.75 , $R_1 = 0.75 D_A$ is required in Equation (27). We put $R_2 = R_{500}$ in Equation (28), concordant with the radius at which the SPT Y_X is measured. In order to be less dependent on the free parameters involved in the universal pressure profile of $P(r)$ and make the computation more reliable, instead of calculating $Y_{\text{sph}}(R_{500})$ directly by Equation (28), we estimate $Y_{\text{sph}}(R_{500})$ via calculating the ratio of $Y_{\text{sph}}(R_{500})$ to $Y_{\text{cyl}}(0.75 D_A)$ from Equations (27) and (28).

The XMM-Newton X-ray observations of 73 of these SZ effect selected clusters have been performed by SPT collaboration members or various non-SPT small programs, among which 15 clusters were excluded due to their low data quality or low redshift ($z < 0.2$). Thus, a sample of 58 clusters with a redshift range of $0.2 < z < 1.5$ is used for analysis (see Figure 1(b)). The sample has a median mass and redshift of $M_{500} = 4.77 \times 10^{14} M_{\odot}$ and $z_{\text{med}} = 0.45$, respectively, and five clusters lie at $z > 1$. The X-ray observable-mass scaling relations of these clusters were studied in Bulbul et al. (2019), and the details of their XMM-Newton observations, especially Y_X values, can be found in Table 1 of Bulbul et al. (2019). Same as the Planck counterparts, the X-ray observables of the sample were measured at R_{500} .

5. Analysis and Results

In order to constrain the parameters of Equation (26), we minimize the following negative log-likelihood function:

$$-2 \ln L = \sum_{i=1}^N \ln 2\pi\sigma_i^2 + \sum_{i=1}^N \frac{[R_{\text{obs},i} - C(1 - \zeta(\phi - \phi_0))^{-3}]^2}{\sigma_i^2}, \quad (29)$$

where

$$R_{\text{obs},i} = \frac{(Y_{SZ} D_A^2)_i}{Y_{X,i} C_{XSZ}} \quad (30)$$

denotes the observed values of the ratio in Equation (26) for galaxy clusters, N is the total number of clusters, and σ_i is the total uncertainty inherited from the observations $(Y_{SZ} D_A^2)_i$ and $Y_{X,i}$, plus an intrinsic scatter term σ_{int} , that is

$$\sigma_i^2 = \left(\frac{\sigma_{SZ,i}}{Y_{X,i} C_{XSZ}} \right)^2 + \left(\frac{(Y_{SZ} D_A^2)_i \sigma_{X,i}}{Y_{X,i} C_{XSZ}} \right)^2 + \sigma_{\text{int}}^2. \quad (31)$$

where $\sigma_{SZ,i}$ and $\sigma_{X,i}$ denote the uncertainty of $(Y_{SZ} D_A^2)_i$ and $Y_{X,i}$, respectively. The advantage of using the log-likelihood against the commonly used χ^2 criterion is that the log-likelihood function can accommodate the optimization of the intrinsic uncertainty. Thus, for the SPT sample the parameter space to be optimized is $\{C, \zeta, \sigma_{\text{int}}\}$. For the Planck sample, we followed Galli (2013) and set $\sigma_{\text{int}} = 0.17$. So the parameter space of the Planck sample is reduced to $\{C, \zeta\}$, and the objective function of Equation (29) becomes equivalent to the χ^2 criterion. Our experiment shows different cosmological parameters only have

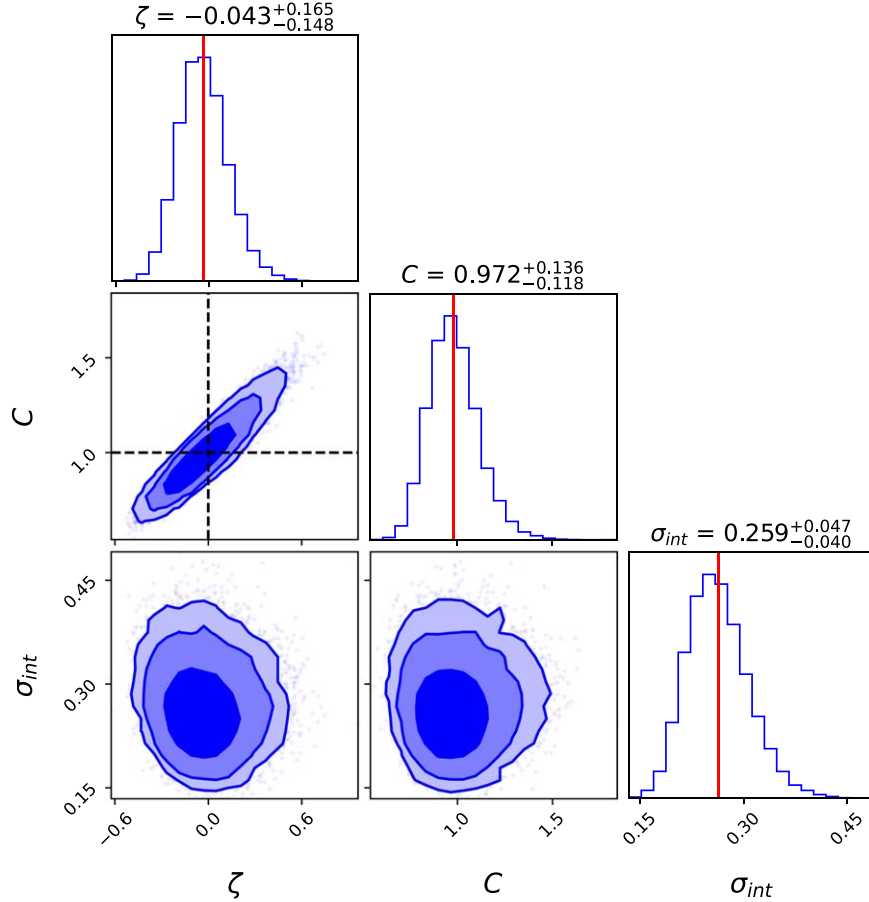


Figure 3. Contours of 1σ , 2σ , and 3σ on the two-dimensional parameter planes and the corresponding one-dimensional marginalized likelihood distributions for the SPT clusters. The red line represents the mean value of each parameter. The dashed lines in the $\zeta - C$ plane mark $\zeta = 0$ and $C = 1$, which represent $\alpha = \alpha_0$ and the isothermality assumption, respectively.

a marginal effect on the result, so we fix the cosmological parameters as $H_0 = 67.4$, $\Omega_m = 0.315$ in the implementation of the quintessence model.

Unlike the Planck cluster sample for which the product of Y_{SZ} and D_A^2 i.e., $Y_{SZ}D_A^2$, is already given as an observational quantity, for SPT data we need to estimate the angular diameter distance to each galaxy cluster via

$$D_A = \frac{1}{1+z} \int_0^z \frac{cdz'}{H(z')}, \quad (32)$$

while $H(z)$ is calculated by the quintessence model (i.e., Equations (5) and (6)).

We maximize the likelihood using the emcee Markov Chain Monte Carlo (MCMC) sampler (Foreman-Mackey et al. 2013). The results on the Planck cluster sample and those on the SPT cluster sample are given in Figures 2 and 3, respectively, which display the 68%, 95%, and 99% confidence level plots along with the marginalized one-dimensional distribution of each parameter. We obtain $\zeta = -0.203^{+0.101}_{-0.099}$, $C = 0.894^{+0.035}_{-0.034}$ from the Planck sample and $\zeta = -0.043^{+0.165}_{-0.148}$, $C = 0.972^{+0.136}_{-0.118}$, and $\sigma_{int} = 0.259^{+0.047}_{-0.040}$ from the SPT sample. We find from Figure 2 that the point ($\zeta = 0$, $C = 1$) is located within the 3σ contour for the Planck sample. Therefore, our results indicate that there is no significant evidence for nonzero ζ , implying no time variation in α . Furthermore, since $C = 1$ holds within 3σ and 1σ for the Planck sample and the SPT sample, respectively, we

conclude that the isothermality assumption of the temperature profile is applicable for both the Planck cluster sample and the SPT cluster sample. It seems that the intrinsic uncertainty of the SPT data ($\sigma_{int} = 0.259$) is heavier than that of the Planck data ($\sigma_{int} = 0.17$). Considering they stem from different analysis methods, this conclusion needs further validation.

6. Conclusions

We explore the possible time variation of the fine structure constant α based on the scaling relation $Y_{SZ}D_A^2/C_{XVZ}Y_X$ calculated from galaxy cluster measurements. Following Colaço et al. (2019), this ratio depends on the fine structure constant through the Thompson cross-section and is also affected by the violation of CDDR through the cluster gas mass. Instead of the frequently used runaway dilaton models, we use the quintessence model to provide the theoretical mechanism of generating time-varying α . Different from the runaway dilaton model, for which the redshift dependence of the dilaton field is explicitly approximated by $\phi(z) = 1 - \gamma \ln(1+z)$ at low and intermediate redshifts, the dynamics of the quintessence scalar field is given by an evolution procedure described using Equations (5) and (6). The resulting equality $Y_{SZ}D_A^2/Y_X C_{XVZ} = C(1 - \zeta(\phi - \phi_0))^{-3}$ is derived to link the quintessence field with the cluster observations.

We use the data of two cluster samples to constrain the variation of the fine structure constant. One sample is the observations of 61 galaxy clusters reported by the Planck

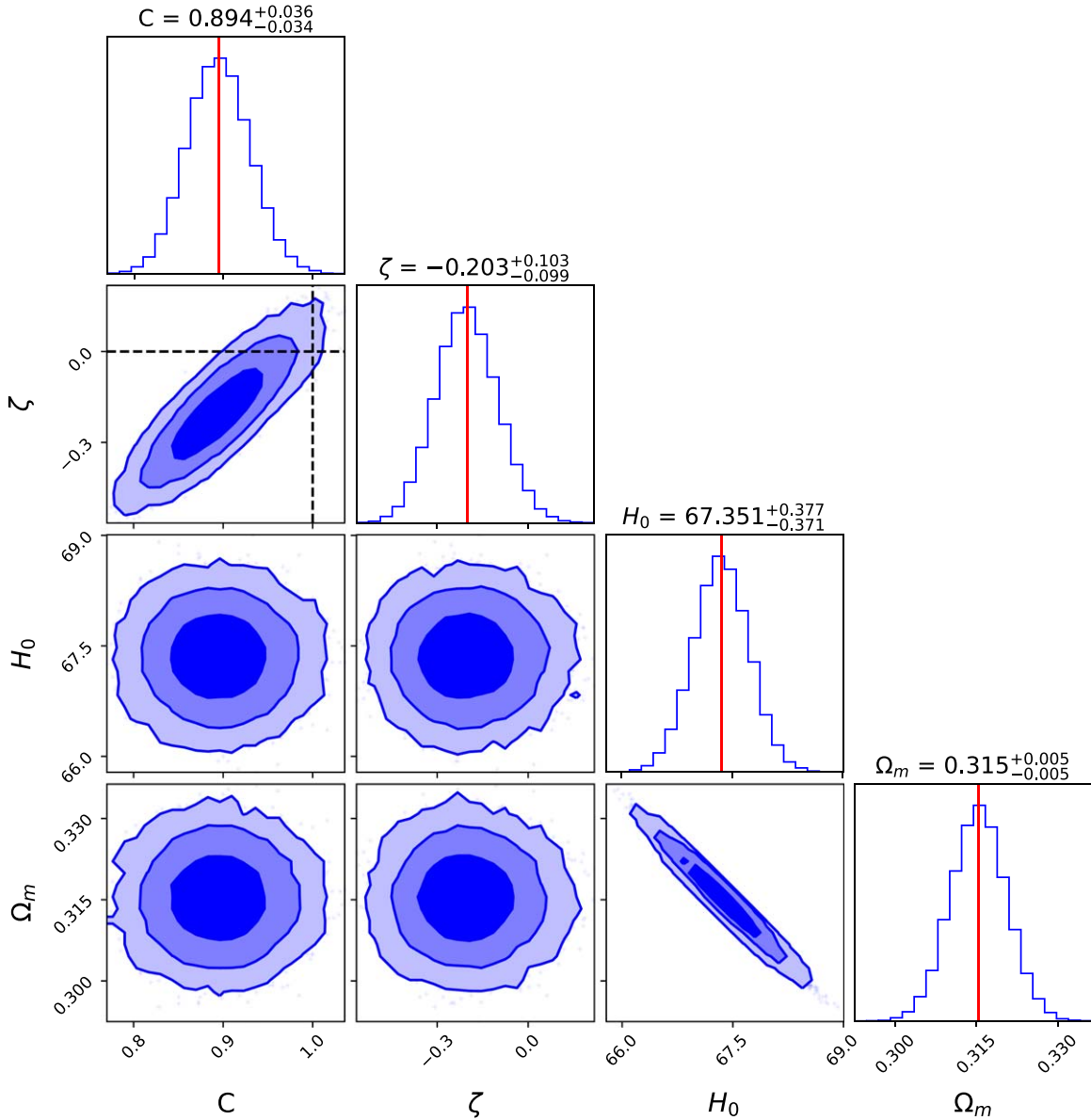


Figure 4. Contours of 1σ , 2σ , and 3σ on the two parameter planes and the corresponding one-dimensional marginalized likelihood distributions for the Planck clusters.

collaboration, and another is the 58 galaxy clusters selected by the SPT–SZ observation. The X-ray counterpart (i.e., Y_X) of both the samples has been observed by the XMM-Newton observations. We give different treatments to the intrinsic uncertainty from the two data sets. For the Planck sample, we set $\sigma_{\text{int}} = 0.17$ directly, while for the SPT sample σ_{int} is taken as a free parameter and the determination of its best value is fused in the optimization procedure. In this way, the intrinsic uncertainty σ_{int} for the SPT sample depends on the dispersion of angular diameter distance D_A and thus is affected by the uncertainties of the cosmological parameters (i.e., H_0 and Ω_m) indirectly. Our analyses show no significant evidence for the fine structure constant α varying with redshift, consistent with previous galaxy cluster-based results (Galli 2013; Colaço et al. 2019; Bora & Desai 2021a, 2021b). The constant C was found to approach unity sufficiently, indicating that the isothermal temperature profile is universal for describing galaxy clusters.

The number of galaxy clusters available is mainly limited by current X-ray observations. For example, among the 516

clusters detected by the SPT–SZ survey, only 73 clusters have corresponding XMM-Newton X-ray observations. The eROSITA (extended Roentgen Survey with an Imaging Telescope Array) satellite, which was launched in 2019, will perform the first imaging all-sky survey in the medium-energy X-ray range and detect 50,000–100,000 galaxy clusters (Hofmann et al. 2017). More detailed and richer observations in the future may let us check whether the conclusion drawn in this paper is still valid in different redshift domains or not. We expect that the problem of α variation would have a better solution by enlarging the galaxy cluster samples.

We thank the anonymous referee for the helpful and constructive feedback. This work was supported by the National Key R & D Program of China (2017YFA0402600), the Natural Science Foundation of Shandong Province, China (Grant NO.ZR2019MA059), and the National Natural Science Foundation of China (grant No. 11929301). Z.Z. is supported in part by NASA grant 15-WFIRST15-0008,

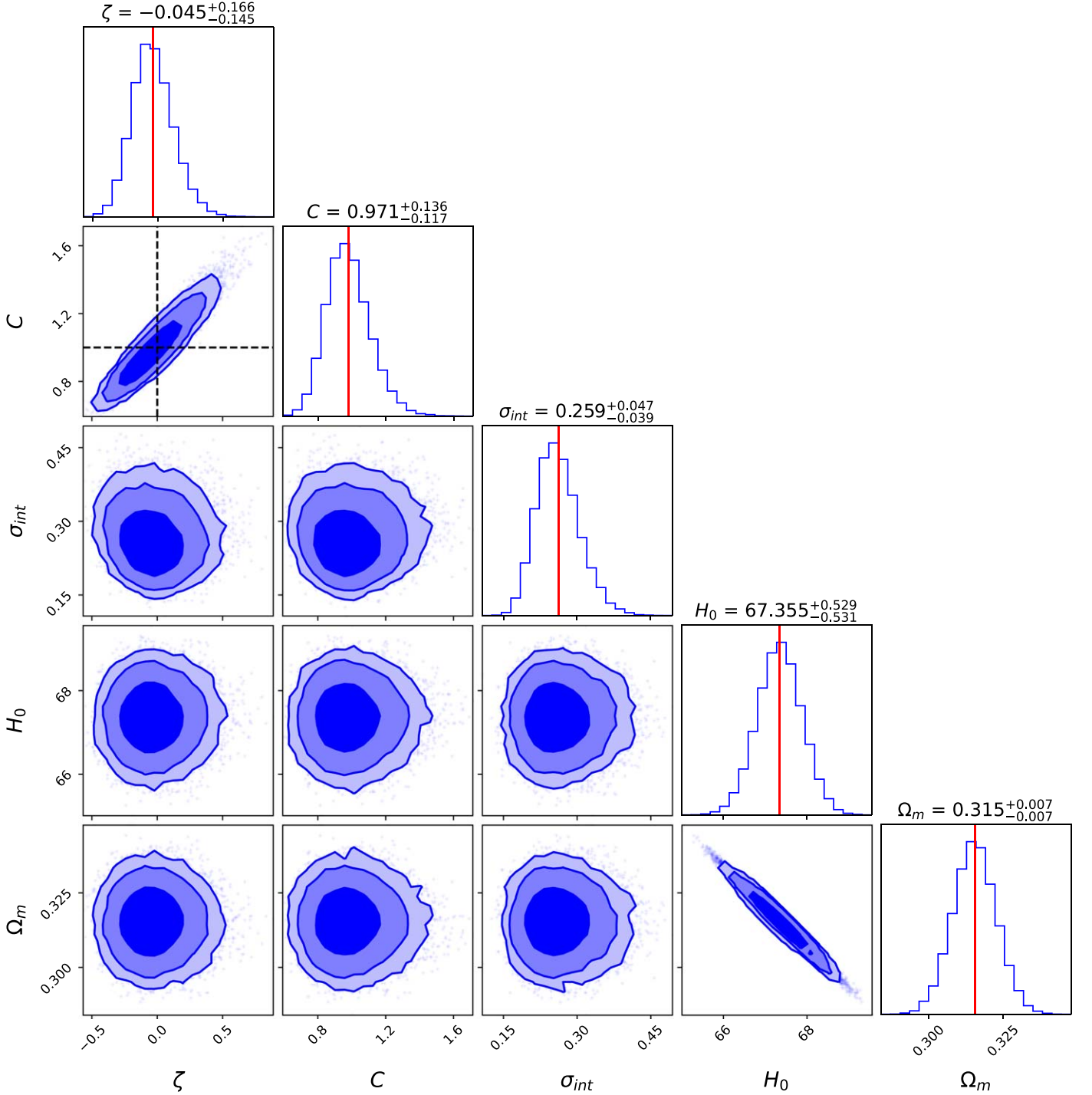


Figure 5. Contours of 1σ , 2σ , and 3σ on the two parameter planes and the corresponding one-dimensional marginalized likelihood distributions for the SPT clusters.

Cosmology with the High Latitude Survey Roman Science Investigation Team (SIT). K.B. acknowledges Department of Science and Technology, Government of India for providing the financial support under the DST-INSPIRE Fellowship program.

Appendix

To demonstrate that the constraints on the time variation of α are insensitive to the cosmological parameters, we repeat the analysis for both data sets treating H_0 and Ω_m as free

parameters. We assume Gaussian bivariate prior distributions on H_0 and Ω_m with the following expression

$$p^{\text{priors}}(x) = \frac{1}{2\pi\sqrt{|\Sigma|}} \times \exp\left(-\frac{1}{2}(x-d)\Sigma^{-1}(x-d)\right), \quad (\text{A1})$$

where $x = \{H_0, \Omega_m\}$, and their mean values $d = \{67.36, 0.3153\}$ and covariance matrix $\Sigma = \begin{pmatrix} 0.287 & -3.89 \times 10^{-3} \\ -3.89 \times 10^{-3} & 5.37 \times 10^{-5} \end{pmatrix}$ are

derived from the CosmoMC chains of Planck 2018 TT,TE,EE +lowE+lensing (Chen et al. 2019). We get $C = 0.894_{-0.034}^{+0.036}$ and $\zeta = -0.202_{-0.101}^{+0.103}$ for the Planck clusters (see Figure 4) and $\zeta = -0.045_{-0.145}^{+0.166}$, $C = 0.971_{-0.117}^{+0.136}$, and $\sigma_{\text{int}} = 0.259_{-0.039}^{+0.047}$ for the SPT clusters (see Figure 5). One can see that compared to the results obtained with fixed H_0 and Ω_m , the difference between the both analyses is insignificant.

ORCID iDs

Zhi-E Liu (刘志娥)  <https://orcid.org/0000-0003-3153-1296>
Tong-Jie Zhang (张同杰)  <https://orcid.org/0000-0002-1596-529X>

Zhong-Xu Zhai (翟忠旭)  <https://orcid.org/0000-0001-7984-5476>

Kamal Bora  <https://orcid.org/0000-0002-6372-9363>

References

- Ade, P. A. R., Aghanim, N., Planck Collaboration, et al. 2011a, *A&A*, **536**, A8
Ade, P. A. R., Aghanim, N., Planck Collaboration, et al. 2011b, *A&A*, **536**, A11
Arnaud, M., Pratt, G., Piffaretti, R., et al. 2010, *A&A*, **517**, A92
Barrow, J. D. 1987, *PhRvD*, **35**, 1805
Barrow, J. D., & Graham, A. A. H. 2013, *PhRvD*, **88**, 103513
Barrow, J. D., & Li, B. 2008, *PhRvD*, **78**, 083536
Barrow, J. D., & Lip, S. Z. W. 2012, *PhRvD*, **85**, 023514
Barrow, J. D., Magueijo, J., & Sandvik, H. B. 2002a, *PhRvD*, **66**, 043515
Barrow, J. D., & Mota, D. F. 2003, *CQGra*, **20**, 2045
Barrow, J. D., Sandvik, H. B., & Magueijo, J. 2002b, *PhRvD*, **65**, 063504
Barrow, J. D., & Tipler, F. J. 1986, *The Anthropic Cosmological Principle* (Oxford: Oxford Univ. Press)
Bekenstein, J. D. 1982, *PhRvD*, **25**, 1527
Berengut, J. C., Flambaum, V. V., Ong, A., et al. 2013, *PhRvL*, **111**, 010801
Bleem, L. E., Stalder, B., de Haan, T., et al. 2015, *ApJS*, **216**, 27
Bocquet, S., Dietrich, J. P., Schrabback, T., et al. 2019, *ApJ*, **878**, 55
Bora, K., & Desai, S. 2021a, *JCAP*, **02**, 012
Bora, K., & Desai, S. 2021b, *JCAP*, **2021**, 052
Bulbul, E., Chiu, I. N., Mohr, J. J., et al. 2019, *ApJ*, **871**, 50
Carlstrom, J. E., Ade, P. A. R., Aird, K. A., et al. 2011, *PASP*, **123**, 568
Chand, H., Srianand, R., Petitjean, P., & Aracil, B. 2004, *A&A*, **417**, 853
Chen, G., & Ratra, B. 2011, *PASP*, **123**, 1127
Chen, L., Huang, Q.-G., & Wang, K. 2019, *JCAP*, **02**, 028
Chodos, A., & Detweiler, S. 1980, *PhRvD*, **21**, 2167
Clara, M. T., & Martins, C. J. A. P. 2020, *A&A*, **633**, L11
Colaço, L. R., Gonzalez, J. E., & Holanda, R. F. L. 2021a, *EPJC*, **81**, 533
Colaço, L. R., Holanda, R. F. L., & Silva, R. 2021b, *EPCJ*, **81**, 822
Colaço, L. R., Holanda, R. F. L., Silva, R., & Alcaniz, J. S. 2019, *JCAP*, **03**, 014
Copeland, E. J., Nunes, N. J., & Pospelov, M. 2004, *PhRvD*, **69**, 023501
Damour, T., & Dyson, F. 1996, *NuPhB*, **480**, 37
Desai, S., Armstrong, R., Mohr, J. J., et al. 2012, *ApJ*, **757**, 83
Dirac, P. 1937, *Natur*, **139**, 323
Dodelson, S., & Schmidt, F. 2020, *Modern Cosmology* (2nd ed.; New York: Academic)
Farajollahi, H., & Salehi, A. 2012, *JCAP*, **2012**, 041
Foreman-Mackey, D., Hogg, D. W., Lang, D., & Goodman, J. 2013, *PASP*, **125**, 306
Fowler, J. W., Niemack, M. D., Dicker, S. R., et al. 2007, *ApOpt*, **46**, 3444
Galli, S. 2013, *PhRvD*, **87**, 123516
Gamow, G. 1967, *PhRvL*, **19**, 759
Goncalves, R. S., Holanda, R. F. L., & Alcaniz, J. S. 2012, *MNRAS*, **420**, L43
Hart, L., & Chluba, J. 2018, *MNRAS*, **474**, 1850
Hees, A., Do, T., Roberts, B. M., et al. 2020, *PhRvL*, **124**, 081101
Hees, A., Minazzoli, O., & Larena, J. 2014, *PhRvD*, **90**, 124064
Hofmann, F., Sanders, J. S., Clerc, N., et al. 2017, *A&A*, **606**, A118
Holanda, R. F. L., Busti, V. C., Colaço, L. R., & Landau, J. S. A. S. J. 2016a, *JCAP*, **08**, 055
Holanda, R. F. L., Colaço, L. R., Gonçalves, R. S., & Alcaniz, J. S. 2017, *PhLB*, **767**, 188
Holanda, R. F. L., Landau, S. J., Alcaniz, J. S., Sánchez, G. I. E., & Busti, V. C. 2016b, *JCAP*, **2016b**, 047
Iocco, F., Mangano, G., Miele, G., Pisanti, O., & Serpico, P. D. 2009, *PhR*, **472**, 1
King, J. A., Webb, J. K., Murphy, M. T., et al. 2012, *MNRAS*, **422**, 3370
Kolb, E. W., Perry, M. J., & Walker, T. P. 1986, *PhRvD*, **33**, 869
Krauss, A. V., Vikhlinin, A., & Nagai, D. 2006, *ApJ*, **650**, 128
Lamoreaux, S. K., & Torgerson, J. R. 2004, *PhRvD*, **69**, 12170
Mantz, A., Allen, S. W., Ebeling, H., Rapetti, D., & Drlica-Wagner, A. 2010, *MNRAS*, **406**, 1773
Marciano, W. J. 1984, *PhRvL*, **52**, 489
Marra, V., & Rosati, F. 2005, *JCAP*, **5**, 011
Martins, C. J. A. P. 2017, *RPPH*, **80**, 126902
Morel, L., Yao, Z., Cladé, P., & Guellati-Khélifa, S. 2020, *Natur*, **588**, 61
Mosquera, M. E., & Civitaresse, O. 2013, *A&A*, **551**, A122
Murphy, M., Webb, J., Flambaum, V., et al. 2001a, *MNRAS*, **327**, 1244
Murphy, M., Webb, J., Flambaum, V., et al. 2001b, *MNRAS*, **327**, 1208
Murphy, M., Webb, J., Flambaum, V., Prochaska, J., & Wolfe, A. 2001c, *MNRAS*, **327**, 1237
Murphy, M. T., Flambaum, V. V., Webb, J. K., et al. 2004, in *Lecture Notes in Physics, Astrophysics, Clocks and Fundamental Constants*, ed. S. G. Karshenboim & E. Peik, 648 (Berlin: Springer), 131
Murphy, M. T., Webb, J. K., & Flambaum, V. V. 2003, *MNRAS*, **345**, 609
Murphy, M. T., Webb, J. K., & Flambaum, V. V. 2007, *PhRvL*, **99**, 239001
Murphy, M. T., Webb, J. K., & Flambaum, V. V. 2008, *MNRAS*, **384**, 1053
O'Bryan, J., Smidt, J., Bernardis, F. D., & Cooray, A. 2015, *ApJ*, **798**, 18
Padmanabhan, T. 2003, *PhR*, **380**, 235
Park, C.-G., & Ratra, B. 2019, *Ap&SS*, **364**, 134
Peebles, P. J. E., & Ratra, B. 1988, *ApJ*, **325**, L17
Piffaretti, R., Arnaud, M., Pratt, G., Pointecouteau, E., & Melin, J.-B. 2011, *A&A*, **534**, A109
PLANCK Collaboration 2015, *A&A*, **580**, A22
Planck Collaboration 2020, *A&A*, **641**, A6
Samushia, L., & Ratra, B. 2006, *ApJ*, **650**, L5
Samushia, L., & Ratra, B. 2009, *ApJ*, **701**, 1373
Sandvik, H. B., Barrow, J. D., & Magueijo, J. 2002, *PhRvL*, **88**, 031302
Saro, A., Bocquet, S., Rozo, E., et al. 2015, *MNRAS*, **454**, 2305
Song, J., Zenteno, A., Stalder, B., et al. 2012, *ApJ*, **761**, 22
Srianand, R., Chand, H., Petitjean, P., & Aracil, B. 2004, *PhRvL*, **92**, 121302
Sunyaev, R. A., & Zel'dovich, Y. B. 1972, *CoASP*, **4**, 173
Teller, E. 1948, *PhRv*, **73**, 801
Uzan, J.-P. 2003, *RvMP*, **75**, 403
Uzan, J.-P. 2011, *LRR*, **14**, 2
Wang, K., & Chen, L. 2020, *EPJC*, **80**, 570
Webb, J. K., Flambaum, V. V., Churchill, C. W., Drinkwater, M. J., & Barrow, J. D. 1999, *PhRvL*, **82**, 884
Webb, J. K., King, J. A., Murphy, M. T., et al. 2011, *PhRvL*, **107**, 191101
Webb, J. K., Murphy, M. T., Flambaum, V. V., et al. 2001, *PhRvL*, **87**, 091301